Biochemical and Biophysical Research Communications 671 (2023) 357–365

Contents lists available at ScienceDirect

Biochemical and Biophysical Research Communications

journal homepage: www.elsevier.com/locate/ybbrc

High-mobility group box-1 peptide ameliorates bronchopulmonary dysplasia by suppressing inflammation and fibrosis in a mouse model

Takeya Hara [a], Takashi Shimbo [b, d], Tatsuo Masuda [d], Tomomi Kitayama [b, c], Makoto Fujii [d, e], Morifumi Hanawa [c], Kazuha Yokota [c], Masayuki Endo [a, d, e, *], Takuji Tomimatsu [a], Tadashi Kimura [a], Katsuto Tamai [b, **]

[a] Department of Obstetrics and Gynecology, Graduate School of Medicine, Osaka University, Suita, Osaka, Japan
[b] Department of Stem Cell Therapy Science, Graduate School of Medicine, Osaka University, Suita, Osaka, Japan
[c] StemRIM Inc., Ibaraki, Osaka, Japan
[d] StemRIM Institute of Regeneration-Inducing Medicine, Osaka University, Suita, Osaka, Japan
[e] Department of Children's and Women's Health, Division of Health Science, Graduate School of Medicine, Osaka University, Suita, Osaka, Japan

ARTICLE INFO

Article history:
Received 30 May 2023
Accepted 8 June 2023
Available online 9 June 2023

Keywords:
Bronchopulmonary dysplasia
Chronic lung disorder
HMGB1
Peptide
Mesenchymal stem cell
Single-cell RNA sequencing

ABSTRACT

Background: This study aimed to examine the effect of the HMGB1 peptide on Bronchopulmonary dysplasia (BPD)-related lung injury in a mouse model.
Results: HMGB1 peptide ameliorates lung injury by suppressing the release of inflammatory cytokines and decreasing soluble collagen levels in the lungs. Single-cell RNA sequencing showed that the peptide suppressed the hyperoxia-induced inflammatory signature in macrophages and the fibrotic signature in fibroblasts. These changes in the transcriptome were confirmed using protein assays.
Conclusion: Systemic administration of HMGB1 peptide exerts anti-inflammatory and anti-fibrotic effects in a mouse model of BPD. This study provides a foundation for the development of new and effective therapies for BPD.

1. Introduction

Bronchopulmonary dysplasia (BPD) is a chronic lung disease that typically affects infants with a birth weight below 1500 g [1], a group that includes approximately 40% of preterm infants [2]. It is associated with significant mortality in neonatal intensive care unit [3,4]. Additionally, survivors are at increased risk of respiratory illnesses and neurodevelopmental disorders compared to healthy infants [5–7]. The etiology of BPD is multifactorial; however, inflammation and trauma observed in all cases of BPD in preterm infants is induced by supplemental oxygen and invasive ventilation, which can eventually cause interstitial fibrosis in the lungs [8]. Fibrosis and impaired alveolarization are important histopathological characteristics in patients with BPD [9].

Although surfactant replacement therapies, corticosteroids, and non-invasive respiratory support are common strategies for managing BPD-related lung injury, they have limited efficacy [10]. New approaches, particularly with mesenchymal stem cells (MSCs), show promise as curative therapies [11,12]. In rodent models of BPD, MSC administration improves alveolarization and ameliorates pulmonary hypertension, lung inflammation, fibrosis, angiogenesis, and apoptosis [12]. However, the clinical application of MSC therapy is hampered by difficulties in preparing large numbers of MSCs of consistent quality [13].

Previously, we have shown that high-mobility group box 1 (HMGB1) induces regeneration by activating platelet-derived growth factor receptor alpha-positive bone marrow MSCs (PDGFRα$^+$ BM-MSCs) [14,15]. HMGB1-induced circulating PDGFRα$^+$ BM-MSCs exhibited regenerative activity in a mouse model of recessive dystrophic epidermolysis bullosa [14]. Our previous study

Abbreviations: BPD, bronchopulmonary dysplasia; MSC, mesenchymal stem cell; MLI, mean linear intercept; RAC, radial alveolar count; HMGB1, high-mobility group box-1; DEG, differentially expressed gene; Sox9, sry-box transcription factor 9; BM-MSC, bone marrow-mesenchymal stem cell; PDGFRα, platelet-derived growth factor receptor alpha-positive; UMAP, uniform manifold approximation and projection.

* Corresponding author. Department of Children's and Women's Health, Graduate School of Medicine, Division of Health Science, Osaka University, Yamadaoka 1-7, Suita, Osaka, 565-0871, Japan.
** Corresponding author. Yamadaoka 2-2, Suita, Osaka, 565-0871, Japan.
E-mail addresses: endo@gyne.med.osaka-u.ac.jp (M. Endo), tamai@gts.med.osaka-u.ac.jp (K. Tamai).

https://doi.org/10.1016/j.bbrc.2023.06.032
0006-291X/

showed that the domain that induces MSCs differentiation resides within the A-box of HMGB1. A human MSC mobilization domain was generated as an HMGB1 fragment comprising A-box and excluding B-box, which causes systemic inflammation [16–18].

This study aimed to examine the effects of systemic administration of the HMGB1 peptide on alveolarization and lung fibrosis in a mouse model of BPD.

2. Materials and methods

2.1. Animal model

All animal procedures were approved by the Animal Committee of Osaka University Graduate School of Medicine (approval number: 03-023-001). All authors complied with the ARRIVE guidelines.

Time-dated pregnant C57BL/6 mice were purchased from CLEA Japan (Tokyo, Japan) on gestation days E14–E15. Animals were housed in individual cages with 12 h light-dark cycles. A standard rodent diet and water were provided ad libitum. Within 12 h of birth, the newborn pups were pooled and randomly allocated to three experimental groups: normoxic conditions with systemic normal saline administration (RA + NS; n = 14), hyperoxic conditions with systemic normal saline administration (O_2+NS; n = 14), and hyperoxic conditions with systemic HMGB1 peptide administration (O_2 + HMGB1; n = 14). Pups in the hyperoxic treatment groups were housed in chambers with 90% oxygen from birth to postnatal day 14 with a brief interruption for husbandry tasks (<10 min/day). The oxygen levels were monitored using a ProOx P110 monitor (Bio-Spherix, Redfield, NY, US). Each nursing dam was assigned seven pups to standardize the nutritional intake. The dams were rotated between hyperoxic and normoxic litters every 24 h to avoid oxygen toxicity. Pups were treated with the HMGB1 peptide or normal saline (control) on postnatal days 4, 8, and 12. As previously described, body weights were measured on postnatal days 4, 8, 12, and 14, without distinguishing between males and females [19]. Mouse pups were euthanized using 2–5% isoflurane inhalation anesthesia on postnatal day 14 for detailed evaluation.

2.2. HMGB1 peptide

As previously reported [16–18,20], StemRIM (Osaka, Japan) used solid-state synthesis to produce HMGB1 peptides from the MSC mobilization domain of human HMGB1. The synthetic HMGB1 peptide was dissolved in distilled water at a concentration of 1 mg/mL prior to systemic administration.

2.3. Systemic administration of HMGB1 peptide or normal saline

Glass needles (diameter: 130 μm) for systemic administration were created using a puller and grinder. HMGB1 peptide or normal saline (each 5 mL/kg/day) was administered on postnatal days 4, 8, and 12 under isoflurane anesthesia [21,22]. On postnatal day 4, HMGB1 peptide were administered via the temporal vein. On postnatal days 8 and 12, a skin incision was made to expose the facial vein for the injection. After the injection, the pups were warmed and returned to their cages.

2.4. Tissue preparation

The pups were euthanized on postnatal day 14 using isoflurane. The chest and abdomen were opened to cut the aorta and vena cava. Lung tissues were harvested for morphometric and biochemical analyses. For morphometric analysis, the lungs were fixed for 5 min at 20 cm H_2O hydrostatic pressure with 4% paraformaldehyde and kept in solution for 24 h at room temperature before being embedded in paraffin.

2.5. Lung morphometric analysis

Lung morphometric analysis was performed as described previously [23–26]. Briefly, 5 μm-thick paraffin-embedded sections were stained with hematoxylin and eosin. We measured the mean linear intercept (MLI) and radial alveolar count (RAC) to estimate the degree of alveolarization. MLI was calculated as the total length of the lines drawn across the lung section divided by the number of intercepts encountered. Two sections per sample and six non-overlapping high-power fields (× 200) per section were evaluated. The RAC was calculated by drawing a line from each respiratory bronchiole to the nearest connective tissue septum and counting the number of alveoli cut by this line. Two sections per sample and five counts per section were performed.

2.6. Enzyme-linked immunosorbent assay

Frozen right lung samples were homogenized in RIPA buffer (Nacalai Tesque, Kyoto, Japan). Inflammatory cytokines interleukin (IL)-1β levels were measured in the lung using the R&D Mouse Quantikine ELISA kit following the manufacturer's protocol (R&D Systems, Minneapolis, MN, USA).

2.7. Collagen measurements

Collagen measurements were obtained from frozen right lung samples using a soluble collagen assay kit (QuickZyme Bioscience, Leiden, NLD), following the manufacturer's protocol.

2.8. Lung isolation and tissue dissociation for scRNA-seq

The lungs (two mice from each group, on postnatal day 14) were rapidly dissected in RPMI-1640 medium (Nacalai Tesque, Kyoto, Japan) containing 10% fetal bovine serum and finely minced. Tissue pieces were digested using a gentle MACS Dissociator (Miltenyi Biotec, Bergisch Gladbach, Germany). The enzyme mixture contained the following: 50 μL of dispase (5000 U/mL; Corning Life Sciences, Oneonta, NY, US), 100 μL of collagenase (100 mg/mL; Wako, Osaka, Japan), 192 μL of elastase (26 mg/mL; Worthington Biochemical Corporation, Lakewood, NJ, US), 10 μL of DNase I (5 U/μL; Takara, Shiga, Japan), and 4648 μL of RPMI-1640 medium (Nacalai Tesque, Kyoto, Japan) with 2% fetal bovine serum. Dissociated cells were passed through a 70 μm cell strainer and centrifuged at 300×*g* for 5 min. The supernatant was discarded, and the pellet was suspended in red blood cell lysis buffer (BioLegend, San Diego, CA, US).

2.9. Library preparation and scRNA-seq

The live cells were sorted using a BD FACSAria III (Becton Dickinson, NJ, USA). Gene expression libraries were prepared using the Chromium Next GEM Single Cell 3 GEM Library & Gel Bead Kit v3.1 (10 × Genomics, Pleasanton, CA, US). A target of 6000 cells was used to generate libraries. Libraries were sequenced on the NextSeq 2000 platform: read lengths were set to 28 (read 1), 8 (i7), 0 (i5), and 91 (read 2) bases.

3. Bioinformatics

3.1. Processing of raw sequencing reads

Raw sequencing reads from the libraries were processed using 10x Genomics Cell Ranger v5.0.0 aligning the reads to the mm10

build of the mouse genome [27] with default parameters. Doublets were detected and removed using the Python package scrublet [28].

3.2. Data quality control, integration, and clustering

All processing steps were performed in the Monocle3 v0.2.3.0 (R package) (https://cole-trapnell-lab.github.io/monocle3/docs/starting/) [29]. The threshold for the minimum read count per cell was set at 500. The thresholds for the minimum number of genes per cell were 39 (RA group) and 56 (O_2+NS and O_2+HMGB1 groups). All mitochondrial and sex chromosomal genes were excluded from analyses. The preprocess_cds() function was used to normalize gene expression and calculate principal components. The top 15 principal components were used for UMAP embedding. Cell types were annotated using the R package SingleR v1.4.0. Default settings were used for all parameters except for the number of dimensions, which is 15 in preprocess_cds() and resolution = 10^{-5} in cluster_cells().

3.3. Differential expression and functional analyses

The R package edgeR v3.34.0 was used to identify DEGs under hyperoxia or BPD treatment [30]. The inclusion criterion was an expression rate >10% of the cells in the cluster. A false discovery rate (FDR) < 0.05 was considered significant.

Gene set enrichment analysis was performed using enrichR v2.1 (R package) [31]. DEGs (FDR <0.05, $|\log_{10}FC| > 1.5$) were assessed for pathway enrichment using the WikiPathway_2019_Mouse reference.

3.4. Statistical analysis

Data are expressed as mean ± SEM. Survival curves were compared using Kaplan–Meier analysis followed by Bonferroni's multiple comparison test. Differences between groups were compared using the Steel–Dwass test. All data were analyzed using JMP Pro 15 software (SAS Institute, Cary, NC, US). Statistical significance was set at $P < 0.05$. A full summary of the statistical information is provided in Supplementary material 1.

4. Results

4.1. HMGB1 peptide treatment ameliorated BPD

As described in previously, we established a well-characterized mouse model of BPD [12,31,32]. Newborn pups were randomly assigned to one of three experimental groups, with 14 pups per group: normoxic (room air) conditions with systemic normal saline administration (RA + NS group), hyperoxic conditions with systemic normal saline administration (O_2+NS group), or hyperoxic conditions with systemic HMGB1 peptide administration (O_2+HMGB1 group) (Fig. 1a). The survival rate (up to postnatal day 14) in the O_2+NS group was significantly lower than that in the RA + NS group, suggesting respiratory system dysfunction. Mice in the O_2+HMGB1 group showed signs of improved survival (Fig. 1b); however, this result was not statistically significant. HMGB1 peptide treatment also significantly reduced body weight loss caused by hyperoxia (Fig. 1c). Corresponding to these observations, hematoxylin and eosin staining revealed that HMGB1 peptide treatment restored hyperoxia-induced lung damage (Fig. 1d). The elevated MLI and reduced RAC levels in the hyperoxia group were significantly ameliorated by HMGB1 treatment. These data suggest that HMGB1 peptide treatment improved the alveolar structure (Fig. 1e and f).

4.2. HMGB1 peptide treatment inhibits migration of inflammatory cells to the injured lung

We performed scRNA-seq to analyze how the HMGB1 peptide restored lung integrity (Fig. 2a). After conventional quality control and filtering, 6104, 4314, and 7584 cells were recovered from the RA + NS, O_2+NS, and O_2+HMGB1 groups, respectively (Supplementary material 2). We identified 15 cell clusters using marker gene analysis and cell type information from previous studies (Fig. 2b) [33]. Cell population analysis revealed an increase in the number of inflammatory cells, including monocytes, neutrophils, and macrophages in the hyperoxic group. Interestingly, treatment with the HMGB1 peptide decreased the abundance of these inflammatory cells (Fig. 2c).

4.3. HMGB1 peptide treatment caused differential gene expression and suppressed BPD-induced inflammation in macrophage fraction

To gain further insight into how the HMGB1 peptide ameliorated BPD-related lung injury, we performed DEG analysis between the O_2+NS and O_2+HMGB1 groups. HMGB1 peptide treatment resulted in significantly altered gene expression patterns, especially in cluster 1 (representing monocytes, macrophages, and DCs), compared with the control treatment (Fig. 3a). In cluster 1, Gene Ontology analysis indicated that the genes in the IL-1 signaling pathway were enriched in the HMGB1 peptide-treated group, suggesting that the HMGB1 peptide modified the inflammatory status of macrophages (Fig. 3b). The upregulation of IL-1β, which has well-characterized involvement in lung inflammation by hyperoxia was partially reverted by the HMGB1 peptide treatment (Fig. 3c) [34,35]. To further confirm the inflammatory status in the HMGB1 treated lungs, we quantified the protein levels of IL-1β. Whereas the amount of IL-1β increased following hyperoxic treatment, HMGB1 peptide treatment significantly suppressed the upregulation of IL-1β (Fig. 3d). These data confirmed that HMGB1 peptide treatment suppressed the inflammatory signatures in BPD lungs.

4.4. HMGB1 peptide treatment inhibited lung fibrosis

To investigate how HMGB1 peptide affects fibrosis, we isolated and re-clustered lung fibroblasts to include clusters 5 and 8 (Fig. 4a). Cell proportion analysis showed that the proportion of sub-cluster 3 increased under hyperoxia (Fig. 4b). Sub-cluster 3 expressed Acta2, suggesting its role in hyperoxia-induced fibrosis (Fig. 4c). DEG and Gene Ontology analyses of sub-cluster 3 (O_2+HMGB1 vs. O_2+NS) highlighted activation of the fibrosis pathway, further confirming the involvement of sub-cluster 3 in fibrosis. DEG analysis of sub-cluster 3 showed that the expression of Sry-box transcription factor 9 (Sox9), which plays a critical role in the progression of pulmonary fibrosis [36], was downregulated by HMGB1 peptide treatment, suggesting the inhibition of fibrosis (Fig. 4d). To confirm the RNA-seq results, we measured the amount of soluble collagen in the lungs to evaluate the degree of fibrosis. Interestingly, the lungs in the O_2+NS group exhibited markedly elevated soluble collagen levels compared with those in the normoxia group. HMGB1 peptide treatment significantly decreased soluble collagen levels (Fig. 4e).

5. Discussion

In this study, we showed that the systemic administration of HMGB1 peptide ameliorated BPD-related lung injury in a mouse model. scRNA-seq analysis showed that HMGB1 peptide treatment suppressed the production of inflammatory cells, including

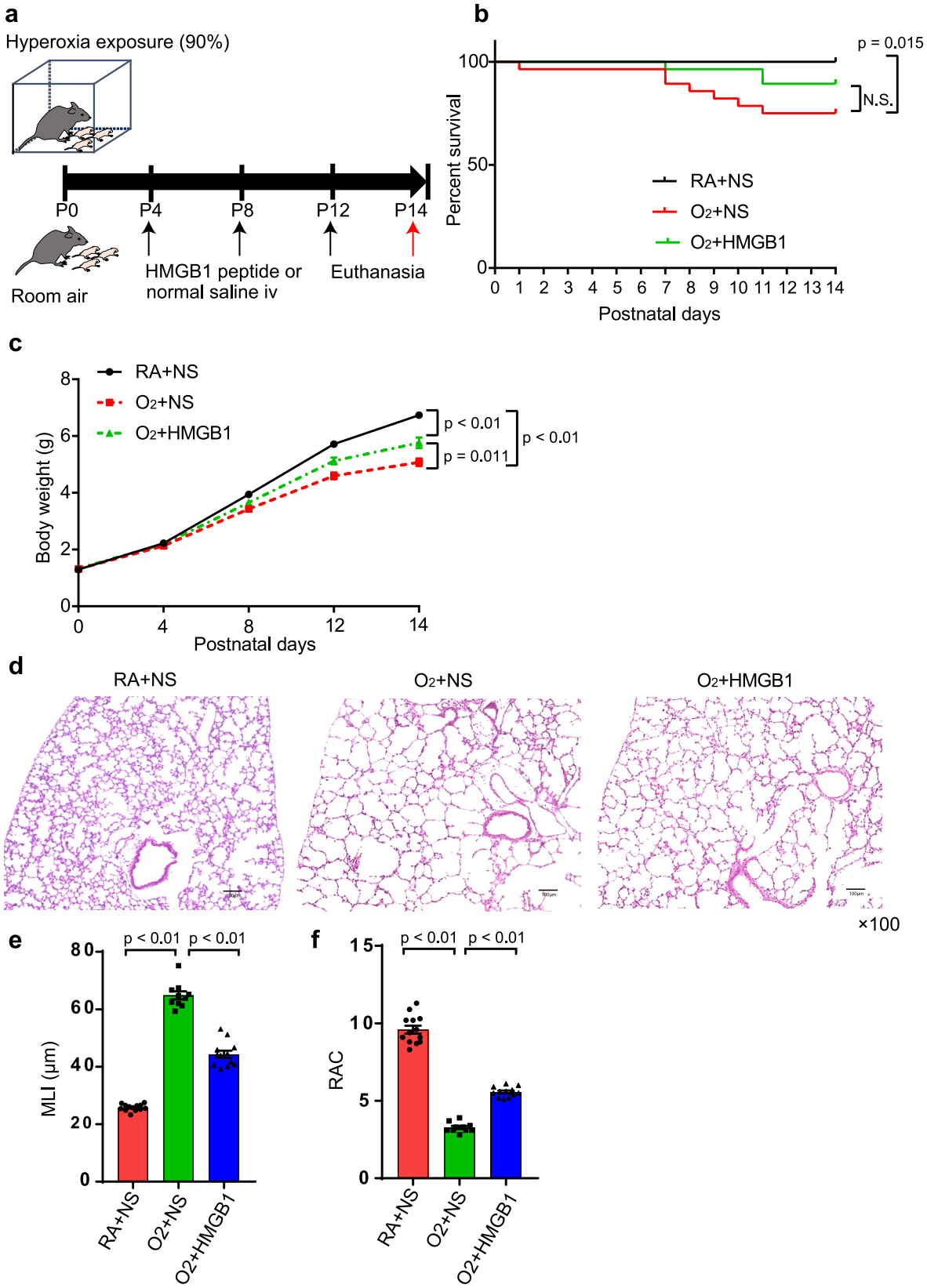

Fig. 1. Effect of HMGB1 treatment on mouse bronchopulmonary dysplasia (BPD) model.
a. Mouse BPD model. From birth until postnatal day (P) 14, normoxic pups were kept in ambient laboratory conditions, and hyperoxic pups were housed in hyperoxic chambers (90% O_2). Pups were administered either HMGB1 peptide or normal saline (control) on P4, 8, and 12. Animals were euthanized on P14 for detailed evaluations. b. Survival curve. Survival curves were summed for the two experiments to make them more equitable (n = 28/group). O_2+NS significantly reduced survival compared to RA + NS (75% vs. 100%, O_2+NS vs. RA + NS; p = 0.015). HMGB1 peptide treatment improved survival; however, the difference was not statistically significant (89% vs. 75%, O_2+HMGB1 vs. O_2+NS; p = 0.436). c. Body weight. Body weights of mice 10–14 at each time point. O_2+NS group was associated with significantly decreased body weight compared to that of RA + NS (4.71 ± 0.20 vs.

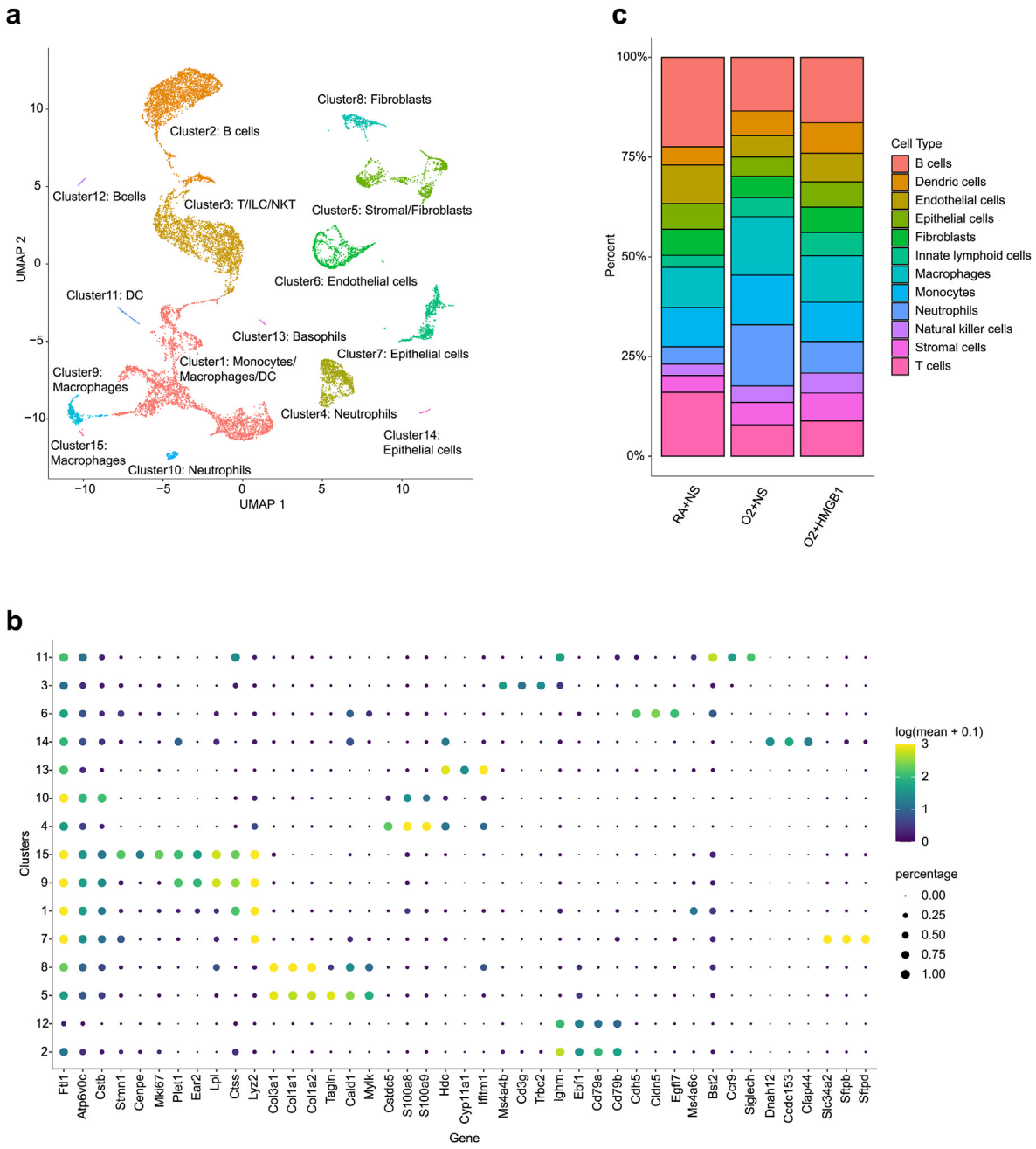

Fig. 2. Single cell RNA-seq on lungs treated with HMGB1 peptide
a. UMAP plot of all scRNA-seq data. b. Marker genes for each cluster. Dot size represents percentage of cells expressing a given gene within the cluster. Intensity of dot color shows mean expression level. c. Cell population analysis of RA + NS, O_2+NS, and O_2+HMGB1. RA + NS, normoxia and normal saline; O_2+NS, hyperoxia and normal saline; O_2+HMGB1, hyperoxia and HMGB1 peptide.

macrophages, neutrophils, and monocytes and reduced inflammatory signatures in the macrophage fraction. At the protein level, a reduced production of IL-1β was detected. Furthermore, HMGB1 peptide treatment decreased the amount of soluble collagen in the lungs of patients with BPD, suggesting a reduction in fibrosis.

Sox9 is a member of the HMGB family, and its role in lung development involves branching morphogenesis of the lung and is highly expressed at the distal tip of the branching epithelium [36,37]. In a recent study, Gajjala et al. reported that myofibroblast-specific Sox9 overexpression augments fibroblast activation and

6.71 ± 0.07 g, O_2+NS (n = 10) vs. RA + NS (n = 14); $p < 0.01$). HMGB1 peptide treatment was associated with a significantly increased body weight compared to that of O_2+NS group (5.47 ± 0.13 vs. 4.71 ± 0.20 g, O_2+HMGB1 (n = 13) vs. O_2 + NS (n = 10); $p = 0.011$). d. The lungs stained with hematoxylin and eosin. e, f. Mean linear intercept (MLI) and radial alveolar count (RAC). O_2+NS was associated with elevated mean linear intercept (MLI; 64.82 ± 1.39 vs. 25.79 ± 0.32 μm, O_2+NS (n = 10) vs. RA + NS (n = 13); $p < 0.01$) and reduced radial alveolar count (RAC; 3.28 ± 0.10 vs. 9.59 ± 0.25, O_2+NS (n = 10) vs. RA + NS (n = 13); $p < 0.01$) compared to RA + NS. HMGB1 peptide treatment significantly ameliorated these effects (MLI: 44.34 ± 1.29 vs. 64.82 ± 1.39 μm, O_2+HMGB1 (n = 12) vs. O_2+NS (n = 10), $p < 0.01$; RAC: 5.57 ± 0.09 vs. 3.28 ± 0.01, O_2+HMGB1 (n = 13) vs. O_2+NS (n = 10), $p < 0.01$). RA + NS, normoxia and normal saline; O_2+NS, hyperoxia and normal saline; O_2+HMGB1, hyperoxia and HMGB1 peptide. Data are expressed as mean ± SEM. Survival curves were compared using Kaplan–Meier analysis followed by Bonferroni's multiple comparison test. Differences between groups were compared using the Steel–Dwass test.

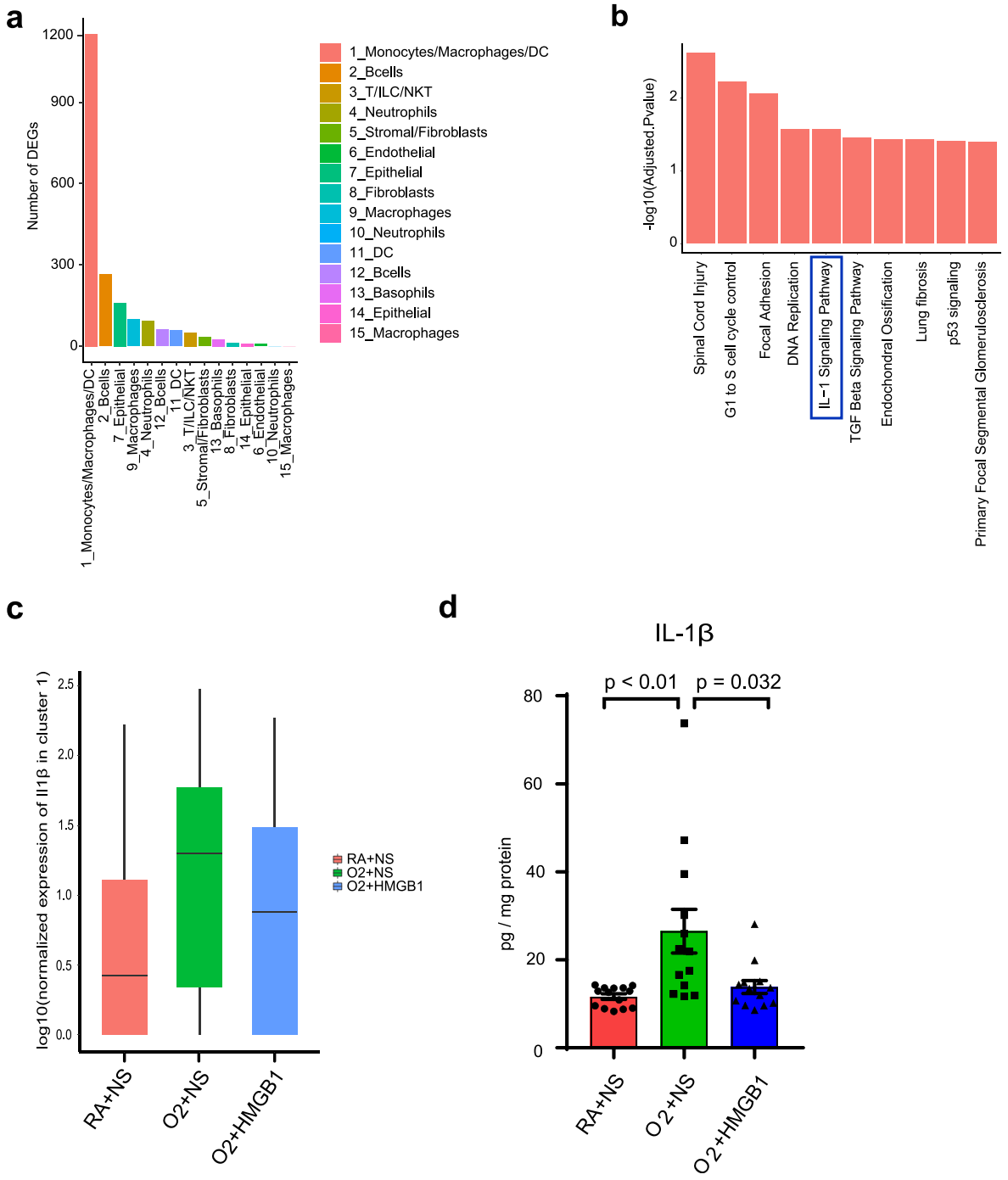

Fig. 3. HMGB1 peptide caused differential gene expression and suppressed BPD-induced inflammation in macrophages.
a. Number of genes in macrophages that are differentially expressed (DEGs) between the O_2+HMGB1 and the O_2+NS groups. b. Gene Ontology analysis for the top 10 enriched biological pathways in macrophages (cluster 1) of O_2+HMGB1 group, compared with the O_2+NS group. c. Box plot showing IL-1β expression in three groups (RA + NS, O_2+NS, and O_2+HMGB1). d. ELISA determined IL-1β level in lungs. O_2+NS significantly elevated lung IL-1β concentrations (26.53 ± 4.96 vs. 11.65 ± 0.61 pg/mg protein, O_2+NS (n = 13) vs. RA + NS (n = 14); $p < 0.01$), but HMGB1 peptide treatment significantly decreased them (13.83 ± 1.46 vs. 26.53 ± 4.96 pg/mg protein, O_2+HMGB1 (n = 13) vs. O_2+NS (n = 13); $p = 0.032$). RA + NS, normoxia and normal saline; O_2+NS, hyperoxia and normal saline; O_2+HMGB1, hyperoxia and HMGB1 peptide. Data are expressed as mean ± SEM. Differences between groups were compared using the Steel–Dwass test.

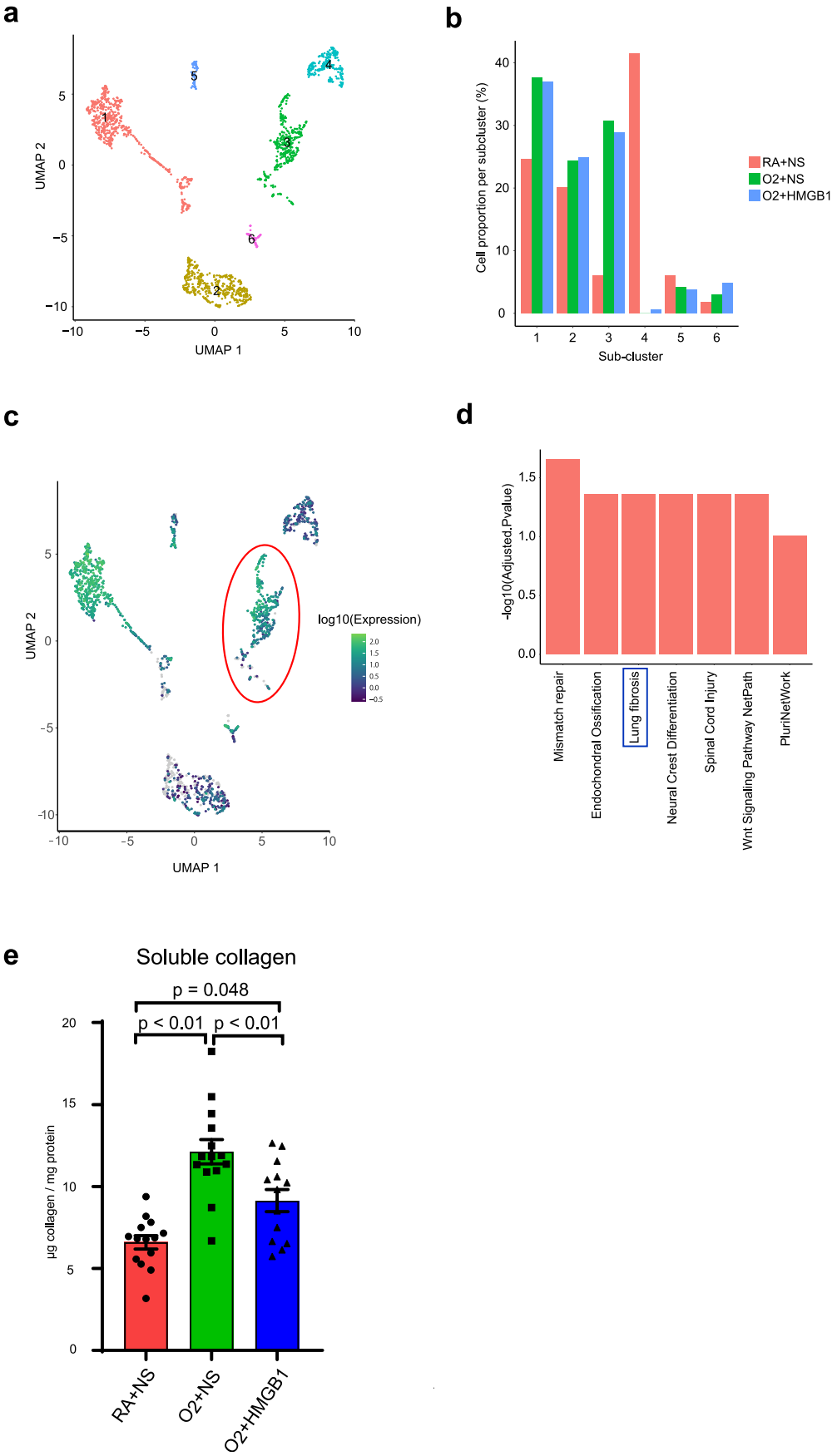

Fig. 4. HMGB1 peptide treatment inhibited lung fibrosis.

a. UMAP plot of fibroblasts. b. Cell proportion analysis in fibroblasts. c. UMAP plot showing Acta2 expression in fibroblasts. Red circle indicates sub-cluster 3. d. Gene Ontology analysis of the top 10 enriched biological pathways in sub-cluster 3 of the myofibroblast fraction in the O_2+HMGB1 group compared to the O_2+NS group. e. Measurement of soluble collagen levels. Lungs in the O_2+NS group exhibited markedly elevated soluble collagen levels compared to lungs in the RA + NS group (12.54 ± 0.67 vs. 6.60 ± 0.41 µg collagen/mg protein, O_2+NS (n = 13) vs. RA + NS (n = 14); $p < 0.01$). HMGB1 peptide treatment significantly decreased these soluble collagen levels (9.14 ± 0.68 vs. 12.54 ± 0.67 µg collagen/mg protein, O_2+HMGB1 (n = 13) vs. O_2+NS (n = 13); $p < 0.01$). RA + NS, normoxia and normal saline; O_2+NS, hyperoxia and normal saline; O_2+HMGB1, hyperoxia and HMGB1 peptide. Data are expressed as mean ± SEM. Differences between groups were compared using the Steel–Dwass test.

lung fibrosis in a mouse model of bleomycin-induced pulmonary fibrosis [36]. In this study, we showed that HMGB1 peptide treatment decreased Sox9 expression at the single-cell level and soluble collagen at the protein level.

Systemic administration of HMGB1 peptide exerted anti-inflammatory and anti-fibrotic effects in a mouse model of BPD. Since there is currently no cure for BPD, our results are extremely important for the development of novel therapies. We expect that this HMGB1 peptide will be applied clinically in the future.

Data statement

All sequencing data used in this study were uploaded to GEO (https://www.ncbi.nlm.nih.gov/geo/; accession number: GSE181497). Information supporting the NGS data can be found in Supplementary Material 2.

Funding

This study was funded by StemRIM and supported by AMED under Grant Number JP19lm0203018 and by JSPS KAKENHI under Grant Numbers JP18K09228, JP21K07796, and JP19H03682. The funding agencies had no role in the collection, analysis, or interpretation of data, in the writing of the report, or in the decision to submit the article for publication.

Declaration of competing interest

The authors declare the following financial interests/personal relationships which may be considered as potential competing interests: Katsuto Tamai reports financial support was provided by StemRIM. Takashi Shimbo reports financial support was provided by StemRIM. Tomomi Kitayama reports financial support was provided by StemRIM. Morifumi Hanawa reports financial support was provided by StemRIM. Kazuha Yokota reports financial support was provided by StemRIM. Katsuto Tamai has patent issued to Osaka university, StemRIM.

Acknowledgements

We thank Mami Nishida., Eiichi Takaki, and Yu-Tung Li for their technical assistance.

Appendix A. Supplementary data

Supplementary data to this article can be found online at https://doi.org/10.1016/j.bbrc.2023.06.032.

References

[1] M.C. Walsh, S. Szefler, J. Davis, et al., Summary proceedings from the bronchopulmonary dysplasia group, Pediatrics 117 (2006) S52–S56, https://doi.org/10.1542/peds.2005-0620I.
[2] B.J. Stoll, N.I. Hansen, E.F. Bell, et al., Trends in care practices, morbidity, and mortality of extremely preterm Neonates, JAMA 314 (2015) 1039–1051, https://doi.org/10.1001/jama.2015.10244, 1993–2012.
[3] E. Khemani, D.B. McElhinney, L. Rhein, et al., Pulmonary artery hypertension in formerly premature infants with bronchopulmonary dysplasia: clinical features and outcomes in the surfactant era, Pediatrics 120 (2007) 1260–1269, https://doi.org/10.1542/peds.2007-0971.
[4] D.H. Kim, H.S. Kim, C.W. Choi, et al., Risk factors for pulmonary artery hypertension in preterm infants with moderate or severe bronchopulmonary dysplasia, Neonatology 101 (2012) 40–46, https://doi.org/10.1159/000327891.
[5] S.V. Jacob, L.C. Lands, A.L. Coates, et al., Exercise ability in survivors of severe bronchopulmonary dysplasia, Am. J. Respir. Crit. Care Med. 155 (1997) 1925–1929, https://doi.org/10.1164/ajrccm.155.6.9196097.
[6] W.H. Northway Jr., R.B. Moss, K.B. Carlisle, et al., Late pulmonary sequelae of bronchopulmonary dysplasia, N. Engl. J. Med. 323 (1990) 1793–1799, https://doi.org/10.1056/NEJM199012273232603.
[7] M.C. Walsh, B.H. Morris, L.A. Wrage, et al., Extremely low birthweight neonates with protracted ventilation: mortality and 18-month neurodevelopmental outcomes, J. Pediatr. 146 (2005) 798–804, https://doi.org/10.1016/j.jpeds.2005.01.047.
[8] A. Bhandari, V. Bhandari, Pathogenesis, pathology, and pathophysiology of pulmonary sequelae of bronchopulmonary dysplasia in premature infants, Front. Biosci. 8 (2003) e370–e380, https://doi.org/10.2741/1060.
[9] W.H. Northway, Observations on bronchopulmonary dysplasia, J. Pediatr. 95 (1979) 815–818, https://doi.org/10.1016/s0022-3476(79)80441-2.
[10] B. Thébaud, K.N. Goss, M. Laughon, et al., Bronchopulmonary dysplasia, Nat. Rev. Dis. Prim. 5 (2019) 78, https://doi.org/10.1038/s41572-019-0127-7.
[11] S. Augustine, W. Cheng, M.T. Avey, et al., Are all stem cells equal? Systematic review, evidence map, and meta-analyses of preclinical stem cell-based therapies for bronchopulmonary dysplasia, Stem Cells Transl. Med. 9 (2020) 158–168, https://doi.org/10.1002/sctm.19-0193.
[12] S. Augustine, M.T. Avey, B. Harrison, et al., Mesenchymal stromal cell therapy in bronchopulmonary dysplasia: systematic review and meta-analysis of preclinical studies, Stem Cells Transl. Med. 6 (2017) 2079–2093, https://doi.org/10.1002/sctm.17-0126.
[13] Y. Morita, H. Ema, H. Nakauchi, Heterogeneity and hierarchy within the most primitive hematopoietic stem cell compartment, J. Exp. Med. 207 (2010) 1173–1182, https://doi.org/10.1084/jem.20091318.
[14] K. Tamai, T. Yamazaki, T. Chino, et al., PDGFRα-positive cells in bone marrow are mobilized by high mobility group box 1 (HMGB1) to regenerate injured epithelia, Proc. Natl. Acad. Sci. U.S.A. 108 (2011) 6609–6614, https://doi.org/10.1073/pnas.1016753108.
[15] E. Aikawa, R. Fujita, Y. Kikuchi, Y. Kaneda, K. Tamai, Systemic high-mobility group box 1 administration suppresses skin inflammation by inducing an accumulation of PDGFRα(+) mesenchymal cells from bone marrow, Sci. Rep. 5 (2015), 11008, https://doi.org/10.1038/srep11008.
[16] T. Goto, S. Miyagawa, K. Tamai, et al., High-mobility group box 1 fragment suppresses adverse post-infarction remodeling by recruiting PDGFRα-positive bone marrow cells, PLoS One 15 (2020), e0230392, https://doi.org/10.1371/journal.pone.0230392.
[17] T. Kido, S. Miyagawa, T. Goto, et al., The administration of high-mobility group box 1 fragment prevents deterioration of cardiac performance by enhancement of bone marrow mesenchymal stem cell homing in the delta-sarcoglycan-deficient hamster, PLoS One 13 (2018), e0202838, https://doi.org/10.1371/journal.pone.0202838.
[18] S. Nojiri, A. Tsuchiya, K. Natsui, et al., Synthesized HMGB1 peptide attenuates liver inflammation and suppresses fibrosis in mice, Inflamm. Regen. 41 (2021) 28, https://doi.org/10.1186/s41232-021-00177-4.
[19] Y. Hu, L. Xie, J. Yu, et al., Inhibition of microRNA-29a alleviates hyperoxia-induced bronchopulmonary dysplasia in neonatal mice via upregulation of GAB1, Mol. Med. 26 (2019) 3, https://doi.org/10.1186/s10020-019-0127-9.
[20] S. Iwai, A. Okada, K. Sasano, et al., Controlled induction of immune tolerance by mesenchymal stem cells transferred by maternal microchimerism, Biochem. Biophys. Res. Commun. 539 (2021) 83–88, https://doi.org/10.1016/j.bbrc.2020.12.032.
[21] H.B. Levene, M. Zhang, C.J. Erb, et al., Method to perform IV injections on mice using the facial vein, J. Neurosci. Methods 164 (2007) 304–307, https://doi.org/10.1016/j.jneumeth.2007.05.007.
[22] S.E. Gombash Lampe, B.K. Kaspar, K.D. Foust, Intravenous injections in neonatal mice, J. Vis. Exp. 93 (2014), e52037, https://doi.org/10.3791/52037.
[23] Y. Luan, L. Zhang, S. Chao, et al., Mesenchymal stem cells in combination with erythropoietin repair hyperoxia-induced alveoli dysplasia injury in neonatal mice via inhibition of TGF-β1 signaling, Oncotarget 7 (2016) 47082–47094, https://doi.org/10.18632/oncotarget.9314.
[24] T.P. Cooney, W.M. Thurlbeck, The radial alveolar count method of Emery and Mithal: a reappraisal 2–Intrauterine and early postnatal lung growth, Thorax 37 (1982) 580–583, https://doi.org/10.1136/thx.37.8.580.
[25] B. Thébaud, F. Ladha, E.D. Michelakis, et al., Vascular endothelial growth factor gene therapy increases survival, promotes lung angiogenesis, and prevents alveolar damage in hyperoxia-induced lung injury: evidence that angiogenesis participates in alveolarization, Circulation 112 (2005) 2477–2486, https://doi.org/10.1161/CIRCULATIONAHA.105.541524.
[26] Y.S. Chang, W. Oh, S.J. Choi, et al., Human umbilical cord blood-derived mesenchymal stem cells attenuate hyperoxia-induced lung injury in neonatal rats, Cell Transplant. 18 (2009) 869–886, https://doi.org/10.3727/096368909X471189.
[27] G.X.Y. Zheng, J.M. Terry, P. Belgrader, et al., Massively parallel digital transcriptional profiling of single cells, Nat. Commun. 8 (2017), 14049, https://doi.org/10.1038/ncomms14049.
[28] S.L. Wolock, R. Lopez, A.M. Klein, Scrublet: computational identification of cell doublets in single-cell transcriptomic data, Cell Syst. 8 (2019) 281–291, https://doi.org/10.1016/j.cels.2018.11.005, e9.
[29] C. Trapnell, D. Cacchiarelli, J. Grimsby, et al., The dynamics and regulators of cell fate decisions are revealed by pseudotemporal ordering of single cells, Nat. Biotechnol. 32 (2014) 381–386, https://doi.org/10.1038/nbt.2859.
[30] M.D. Robinson, D.J. Mccarthy, G.K. Smyth, edgeR: a Bioconductor package for differential expression analysis of digital gene expression data, Bioinformatics 26 (2010) 139–140, https://doi.org/10.1093/bioinformatics/btp616.
[31] C. Nardiello, I. Mižíková, D.M. Silva, et al., Standardisation of oxygen exposure in the development of mouse models for bronchopulmonary dysplasia, Dis.

Model. Mech. 10 (2017) 185–196, https://doi.org/10.1242/dmm.027086.
[32] J. Berger, V. Bhandari, Animal models of bronchopulmonary dysplasia. The term mouse models, Am. J. Physiol. Lung Cell Mol. Physiol. 307 (2014) L936–L947, https://doi.org/10.1152/ajplung.00159.2014.
[33] M. Hurskainen, I. Mižíková, D.P. Cook, et al., Single cell transcriptomic analysis of murine lung development on hyperoxia-induced damage, Nat. Commun. 12 (2021) 1565, https://doi.org/10.1038/s41467-021-21865-2.
[34] S.Y. Ahn, Y.S. Chang, D.K. Sung, et al., Cell type-dependent variation in paracrine potency determines therapeutic efficacy against neonatal hyperoxic lung injury, Cytotherapy 17 (2015) 1025–1035, https://doi.org/10.1016/j.jcyt.2015.03.008.
[35] Y.S. Chang, S.Y. Ahn, H.B. Jeon, et al., Critical role of vascular endothelial growth factor secreted by mesenchymal stem cells in hyperoxic lung injury, Am. J. Respir. Cell Mol. Biol. 51 (2014) 391–399, https://doi.org/10.1165/rcmb.2013-0385OC.
[36] P.R. Gajjala, R.K. Kasam, D. Soundararajan, et al., Dysregulated overexpression of Sox9 induces fibroblast activation in pulmonary fibrosis, JCI Insight 6 (2021), e152503, https://doi.org/10.1172/jci.insight.152503.
[37] B.E. Rockich, S.M. Hrycaj, H.P. Shih, et al., Sox9 plays multiple roles in the lung epithelium during branching morphogenesis, Proc. Natl. Acad. Sci. U.S.A. 110 (2013) E4456–E4464, https://doi.org/10.1073/pnas.1311847110.